New Journal of Physics

The open access journal at the forefront of physics

PAPER

Bulk-boundary quantum oscillations in inhomogeneous Weyl semimetals

Dmitry I Pikulin[1,3] and Roni Ilan[2]

1   Station Q, Microsoft Research, Santa Barbara, CA 93106-6105, United States of America
2   Raymond and Beverly Sackler School of Physics and Astronomy, Tel-Aviv University, Tel-Aviv 69978, Israel
3   Author to whom any correspondence should be addressed.

E-mail: dmpikuli@microsoft.com

Abstract

In a Weyl semimetal, a spatially inhomogeneous Weyl node separation caused by lattice deformations can mimic the action of axial electromagnetic fields. Such fields can locally drive a chiral magnetic effect, a local macroscopic current, in equilibrium. In the present work, we study the interplay of external and intrinsic magnetic fields and explore the fate of bulk boundary oscillations in systems subjected to strain gradients. We show that the emerging intrinsic fields leave distinct hallmarks on the period of the oscillations by modifying the particle trajectories. This makes the oscillations depend on the geometry of the system in an analytically traceable manner. We, therefore, predict that quantum oscillations are a natural way to observe and quantify intrinsic magnetic fields, both of which have not been achieved yet in the solid state.

Band structures of three-dimensional crystalline materials can exhibit non-degenerate band crossings, functioning as monopoles emitting a momentum space equivalent of magnetic flux. These momentum space defects must come in pairs of opposite charges due to periodicity of the Brillouin zone. Electrons in the vicinity of such so-called Weyl nodes can be assigned a quantum number, chirality, determined by the charge of the 'Berry monopole'. The chirality can couple to observable transport phenomena and affect response functions for the system. As the terminology implies, there is a one-to-one correspondence between the effective theory describing these low energy excitations, and the physics of the high energy Weyl fermions. Hence, Weyl semimetals (WSMs), materials hosting such nodes, offer a pathway for realizing relativistic phenomena in $3 + 1$ dimensions, representing a microcosm contained within a solid state sample [1–7].

The consequences of the chiral charges in field theory are well known and celebrated. In particular, the chiral magnetic effect (CME) is a current response from a single specie of Weyl fermions generated along the direction an externally applied magnetic field [1, 8]. The same phenomenon is expected to occur in WSM, due to the structure of the bulk Landau levels developing around the Weyl point: the lowest Landau level disperses in the direction of the field, with a group velocity that is determined by the sign of the topological charge of the nodes. However, the detection of the CME in a solid state system is made complicated by the Nielsen-Ninomiya theorem, dictating that the CME vanishes in equilibrium due to a cancellation of contributions from nodes of opposite chiralities [9–12]. Pair of nodes of opposite chiralities host counter propagating modes that cancel one another, resulting in zero total CME in equilibrium. One can obtain a non cancellation of the CME only in non-equilibrium conditions, either through dynamics, or through an imbalance of chiral chemical potentials [13–19].

In stark contrast to the discussion above, a CME arising from pseudo-magnetic fields can be sustained locally even in equilibrium conditions. Since such fields act with an opposite sign on the two types of chiral fermions, their contributions to equilibrium currents are added to one another instead of canceling. The only constraint imposed on such currents, is that they must vanish when integrating over the entire sample [20–22]. This phenomenon is linked to a known fact from classical electromagnetism—bound currents as a result of

inhomogeneous magnetization can flow within a medium so long as the total dissipation-less current vanishes when averaged over the volume of the sample.

Deformed bulk-boundary quantum oscillations in the presence of pseudo-fields

In this work we address an outstanding challenge concerning the physics of WSM by proposing a direct way to detect and quantify the emergence of pseudo-magnetic fields and the resulting pseudo-CME. We achieve this by exploring the effects of inhomogeneities on a known and proven experimental scheme: quantum oscillations due to semiclassical trajectories traversing the bulk and surface of WSM [23–25]. Originally, this striking transport measurement was used to prove the existence of bulk-surface trajectories that result in a coherent periodic motion driven solely by the external magnetic field via the CME. In the present work we show that the addition of pseudo-magnetic fields generated by strain, can deform the bulk quasiparticle trajectories and hence have immediate and quantifiable effects on the period of the oscillations. Moreover, these effects allow for direct extraction of the pseudo-magnetic field magnitude from the experiment.

The emergence of the pseudo-fields in Dirac materials has been shown to have striking consequences in graphene. In WSMs it has recently been claimed to play a key role both in the understanding of the physics of Fermi arcs, as well as in driving an equilibrium CME, or give rise to novel forms of the chiral anomaly in the presence of electric fields. Both in graphene, as well as in WSM, lattice deformations couple to the electronic degrees of freedom as gauge potentials that do not break time-reversal symmetry, but nevertheless result in the formation of Landau levels [26, 27]. Preserving time-reversal symmetry comes about through the coupling of the pseudo-fields with an opposite sign to the two valleys of graphene, or to Weyl points of opposite chiral charges in WSM. While pseudo-fields can emerge via any mechanism that renders the Weyl node positions space dependent, such as lattice deformation or an inhomogeneous magnetization, the emergent pseudo-gauge fields couple to fermions of opposite chirality with an opposite sign [20, 21, 28–34]. Time-reversal preserving pseudo-fields in Weyl-like systems have been recently demonstrated in meta-materials [35].

The principle behind the effect of pseudo-fields on quantum oscillations is simple: quantum oscillations stem from trajectories that traverse the bulk via the dispersion of the lowest Landau level, combined with a semiclassical sliding motion along the arcs at the surface perpendicular to the direction of the field [23, 24]. When fixing the direction of the external magnetic field such trajectories are deformed due to intrinsic magnetic fields. This is because particles in the bulk are forced to move in the direction of the total effective magnetic field felt by the Weyl node, which is a superposition of the two components (external and intrinsic).

Below we derive the relevant formula for the period of the semiclassical oscillations. As we show, deformed trajectories have a strong quantifiable effect on the density of states (DOS) as well as the frequency of oscillations in experimentally available responses (e.g. conductivity). While oscillations in the absence of pseudo-fields are periodic and depend only on the total momentum space enclosed by the Fermi arcs [23, 24], with bulk pseudo-fields the interval between oscillations becomes field-, pseudo-field-, as well as thickness dependent. We support our predictions with numerical simulations performed using a tight-binding model compatible with the physics of Cd_3As_2, a Dirac semimetal on which the original quantum oscillations experiment was performed [25].

Analytic considerations: geometric factors affecting the oscillation period

To make our discussion concrete, consider a film of a WSM. For simplicity, we consider a WSM with a single pair of Weyl nodes, but the analysis straightforwardly generalizes. We take the Weyl node separation $\mathbf{p}_0$ to be along p_x as depicted in figure 1. Then the low energy Hamiltonian is

$$H_0 = \pm v(\mathbf{p} \pm \mathbf{p}_0) \cdot \sigma - \mu_0, \tag{1}$$

where v is the velocity, which we take here to be isotropic (the case of anisotropic velocity is discussed in the Methods section), and μ_0 is the chemical potential offset with respect to the Dirac point. We note that written in this form, $\mathbf{p}_0$ couples to the Hamiltonian as an axial vector potential. When $\mathbf{p}_0$ is a constant, its importance is in the separation of nodes but beyond that it brings about no other interesting additional structure to the Weyl cones, since $\nabla \times \mathbf{p}_0 = 0$. Inhomogeneous strain, however, renders the Weyl node separation space-dependent [20, 21, 31, 36], and may make $\nabla \times \mathbf{p}_0$ non-zero. For simplicity we consider a strain profile that makes $\mathbf{p}_0$ depend linearly on the z coordinate. As we show below, such profile corresponds to a physical strain configuration. In such case we can write the Weyl nodes separation as $\mathbf{p}_0(z) = (b_0 - B_5 z)\hat{y}$. Now, taking the curl of $\mathbf{p}_0(z)$ we can define $\mathbf{B}_5 = 1/e\nabla \times \mathbf{p}_0(x) = B_5\hat{x}$, which is a pseudo-magnetic field that couples to Weyl nodes of opposite chirality with an opposite sign. Therefore, this position-dependent Weyl node separation and, as a result, bulk strain leads to intrinsic pseudo-magnetic fields. We note however, that unlike in the case of regular magnetic field, $\mathbf{p}_0$ is not a gauge-dependent quantity as it is directly observable as a bandstructure parameter [37]. The pseudo-magnetic field breaks the linear Dirac spectrum around each node into Landau
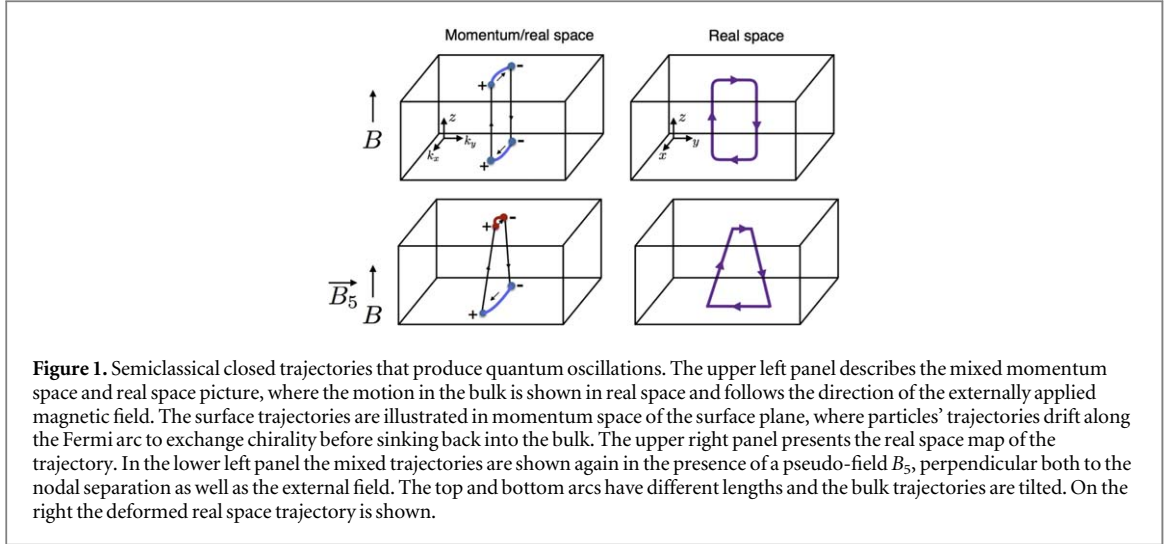
Figure 1. Semiclassical closed trajectories that produce quantum oscillations. The upper left panel describes the mixed momentum space and real space picture, where the motion in the bulk is shown in real space and follows the direction of the externally applied magnetic field. The surface trajectories are illustrated in momentum space of the surface plane, where particles' trajectories drift along the Fermi arc to exchange chirality before sinking back into the bulk. The upper right panel presents the real space map of the trajectory. In the lower left panel the mixed trajectories are shown again in the presence of a pseudo-field B_5, perpendicular both to the nodal separation as well as the external field. The top and bottom arcs have different lengths and the bulk trajectories are tilted. On the right the deformed real space trajectory is shown.

levels, with a dispersion relation

$$\epsilon_n(k_x) = \pm \mathrm{sgn}\,(n) v \sqrt{k_x^2 + 2\ell_{B_5}^{-2}}, \tag{2}$$

$$\epsilon_0(k_x) = -\mathrm{sgn}(B_5) v k_x. \tag{3}$$

Here and later $\ell_{B(B_5)} = \frac{1}{\sqrt{eB(B_5)}}$, $\hbar = 1$. As the pseudo-magnetic field acts oppositely in the two Weyl nodes, for the given node configuration the chirality of the lowest Landau level is the product of the sign of B_5 in that node and the corresponding Weyl node chirality.

We now turn to the influence of B_5 on the bulk trajectories. Assuming an externally applied field in the z direction, $\mathbf{B} = B\hat{z}$ the total field experienced by a particle with chirality s (with $s = \pm 1$) is

$$\mathbf{B}_s = \mathbf{B} + s\mathbf{B}_5 = B\hat{z} + sB_5\hat{x}. \tag{4}$$

The intrinsic field thus tilts the bulk trajectories from the direction of the external field by an angle $\theta = \tan^{-1} B_5/B$. Hence, the bulk path traversed is of length $L' = L/\cos\theta = L\sqrt{1 + (B_5/B)^2}$, where L is the thickness of the sample.

In order to determine the period of quantum oscillations, we follow the analysis in [24], and derive the phase space quantization condition for the closed quasiparticle trajectories

$$\oint_c \mathbf{p} \cdot \mathbf{dr} = 2\pi(n + \gamma), \tag{5}$$

where γ is a constant offset. According to the discussion above, the integral for the mixed bulk-surface trajectories is broken into two pieces, due to the presence of the intrinsic and external vector potentials, namely the integral is taken over four segments of the trajectories, including the two arcs, and two bulk branches linking the top and the bottom surfaces. See figure 1 for depiction of the trajectories in the mixed real-momentum and purely real spaces. For the arcs, the integral yields

$$\int \mathbf{p} \cdot \mathbf{dr} = e\Phi, \tag{6}$$

where Φ is the total flux enclosed by the real space orbit in the surface plane. If the surface encircled is S, then[38]:

$$\Phi = SB = BS_k \ell_B^4 \tag{7}$$

with S_k the momentum space area enclosed by the arcs. At small chemical potential this area is approximately given by $S_k = k_0(\mu + \mu_0)/v$, where k_0 is the total length of the arcs, μ is the chemical potential measured from the Weyl nodes, μ_0 is the chemical potential offset as discussed in [24] and v the Fermi velocity at the surface which we take to be equal to that of the bulk. Note that in principle, k_0 may depend on B_5: the presence of B_5 in the bulk necessarily means the length of the two arcs on opposite surfaces is inequivalent. Here, we will analyze the simplest case in which strain enhances the arc length on one surface by the same amount it shortens the arc on the opposite surface. Then, the total length of the surface trajectory is not modified by B_5, although B_5 is finite in the bulk. This corresponds to the physical strain, corresponding to bending the WSM field, discussed in [39]. In the Methods section we discuss other cases where changes in the two arcs do not compensate one another.

In the bulk, the trajectory of the particles is parallel to the total magnetic field, so that[4]

$$\int \mathbf{p} \cdot \mathbf{dr} = L\sqrt{1 + (B_5/B)^2}\left(2\mu \Big/ v\right). \tag{8}$$

Defining $L_{\text{eff}} = 2L\sqrt{1 + (B_5/B)^2}$ and summing the two contributions together we have

$$2\pi(n + \gamma) = \mu L_{\text{eff}}/v + eBS_k\ell_B^4. \tag{9}$$

From equation (9) we can obtain our first testable prediction. The positions of the bulk-boundary energy levels represent the points in which the chemical potential fulfills equation (9) and are given by:

$$\epsilon_n \equiv \frac{2\pi(n + \gamma)v - k_0\mu_0 l_B^2}{L_{\text{eff}} + k_0\ell_B^2} \tag{10}$$

and are strongly affected by B_5. Increasing B_5 makes the levels more dense. Furthermore, we can consider quantum oscillations as a function of B or B_5. At $B_5 = 0$, the oscillations' period is $\Delta(1/B) \approx 2\pi e/S_k$. As a small B_5 is introduced, a correction is added to the denominator, $S_k \rightarrow S_k + 2\mu eLB_5^2/vB$, making the oscillations non-periodic, as the separation between peaks becomes magnetic field dependent. Moreover, as opposed to the case of a purely external magnetic field, the separation between peaks is now thickness dependent. In the opposite limit $B_5 \gg B$, we obtain $\Delta(1/B) = 2\pi e/(S_k + 2\mu LB_5/v)$, from which it is clear that that while oscillations are periodic in $1/B$, B_5 decreases the period of oscillations, and makes it depend on the sample thickness.

Thus we obtain our main experimental predictions: closed bulk-boundary trajectories produce peaks in DOS at energies corresponding to the solutions of the equation (10). These can be observed in conductance (Shubnikov-de Haas, SdH) and magnetization (de Haas-van Alphen, dHvA).

Numerical tests: modified DOS

To confirm the validity of the results above and their applicability to realistic materials and conditions we performed numerical simulations of a discretized Hamiltonian applicable to Cd_3As_2 and Na_3Bi Dirac semimetals. In these semimetals we can neglect the spin–orbit coupling, thus we use the basis of a single spin, $|s\uparrow, p\uparrow\rangle$. In this basis the continuous Hamiltonian reads:

$$H(k) = \begin{pmatrix} E_s & Ap_+ \\ Ap_- & E_p \end{pmatrix}, \tag{11}$$

where:

$$E_s = e_s + m_{s\perp}p_x^2 + m_{s\parallel}p_\parallel^2; \tag{12}$$

$$E_p = e_p + m_{p\perp}p_x^2 + m_{p\parallel}p_\parallel^2, \tag{13}$$

$p_\pm = p_y \pm ip_z$, $p_\parallel = (p_y, p_z)$, and the parameters used are summarized in figure 2. Note that we use the particle-hole symmetric version of the model for simplicity ($E_p = -E_s$). For this model we identify: distance between the Weyl nodes $\mathbf{p}_0 = \left(\sqrt{\frac{e_s}{m_{s\perp}}}, 0, 0\right)$, and velocities around the Weyl points, $v_\perp = 2\sqrt{e_s m_{s\perp}}$, and $v_\parallel = A$. For the purpose of our simulations we set $v_\perp = v_\parallel$ by changing A. This makes comparison to (10) straightforward.

We use the same procedure as in [39] to introduce the B_5 field according to the displacement vector:
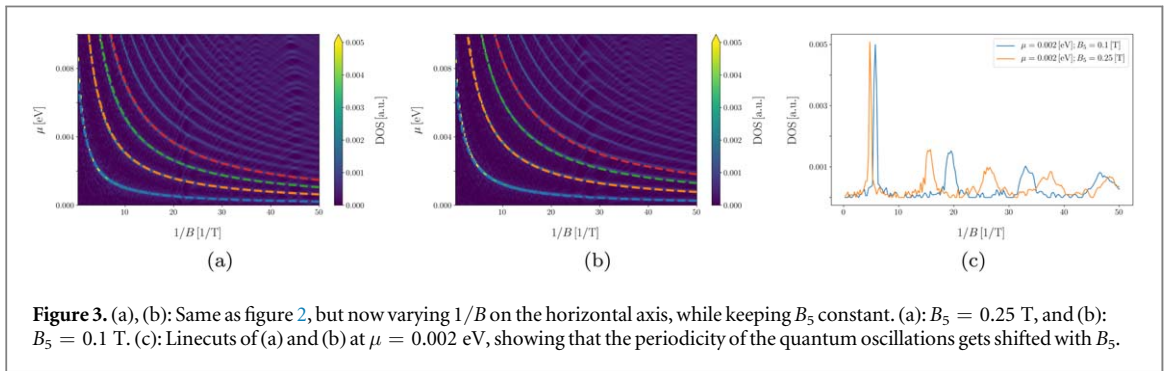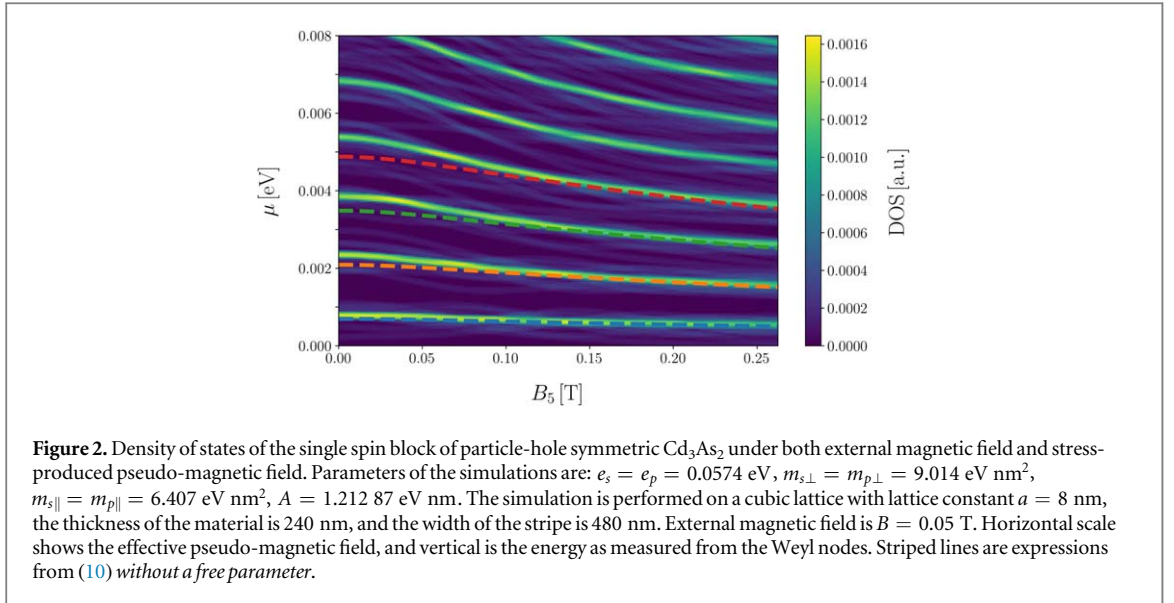
$$\mathbf{u} = (2\alpha xz, 0, 0), \tag{14}$$

where α controls the strength of the strain. From this we compute the elements of the symmetric strain tensor $u_{ij} = (\partial_i u_j + \partial_j u_i)/2$. Then $u_{13} = 2\alpha x$, and $u_{11} = 2\alpha z$ and correspondingly the pseudo-magnetic field generated by the strain. In this model the u_{13} has much smaller contribution to the pseudo-magnetic field than u_{11} due to a small prefactor $(\tilde{a}p_0)^2$, where $\tilde{a}$ is the lattice constant of the material. For Cd_3As_2 this prefactor is $\approx 1/57$ [39]. We thus only use u_{11}, which gives uniform pseudo-magnetic field in y direction of strength $B_5 = 2\alpha\frac{\hbar c}{ea}\cot ap_0$. Such strain corresponds to the modification of hopping in x direction according to:

$$t_x \rightarrow t_x(1 - 2\alpha z). \tag{15}$$

Such modification makes the distance between the Weyl nodes, set by hopping in z direction, position-dependent, in accordance with the definition of B_5 we used above.

---

[4] Generically, the integral $\int \mathbf{p} \cdot \mathbf{dr}$ will also contain another contribution from the dot product of the nodal separation vector $\mathbf{p}_0$ and the external field (see [24]), however, for our choice of directions, this contribution is zero. In addition, the contribution proportional to $\int \mathbf{A} \cdot \mathbf{dr}$ also vanishes, as the bulk trajectories enclose no net flux.

Figure 2. Density of states of the single spin block of particle-hole symmetric Cd_3As_2 under both external magnetic field and stress-produced pseudo-magnetic field. Parameters of the simulations are: $e_s = e_p = 0.0574$ eV, $m_{s\perp} = m_{p\perp} = 9.014$ eV nm^2, $m_{s\parallel} = m_{p\parallel} = 6.407$ eV nm^2, $A = 1.212\,87$ eV nm. The simulation is performed on a cubic lattice with lattice constant $a = 8$ nm, the thickness of the material is 240 nm, and the width of the stripe is 480 nm. External magnetic field is $B = 0.05$ T. Horizontal scale shows the effective pseudo-magnetic field, and vertical is the energy as measured from the Weyl nodes. Striped lines are expressions from (10) *without a free parameter*.

Figure 3. (a), (b): Same as figure 2, but now varying $1/B$ on the horizontal axis, while keeping B_5 constant. (a): $B_5 = 0.25$ T, and (b): $B_5 = 0.1$ T. (c): Linecuts of (a) and (b) at $\mu = 0.002$ eV, showing that the periodicity of the quantum oscillations gets shifted with B_5.

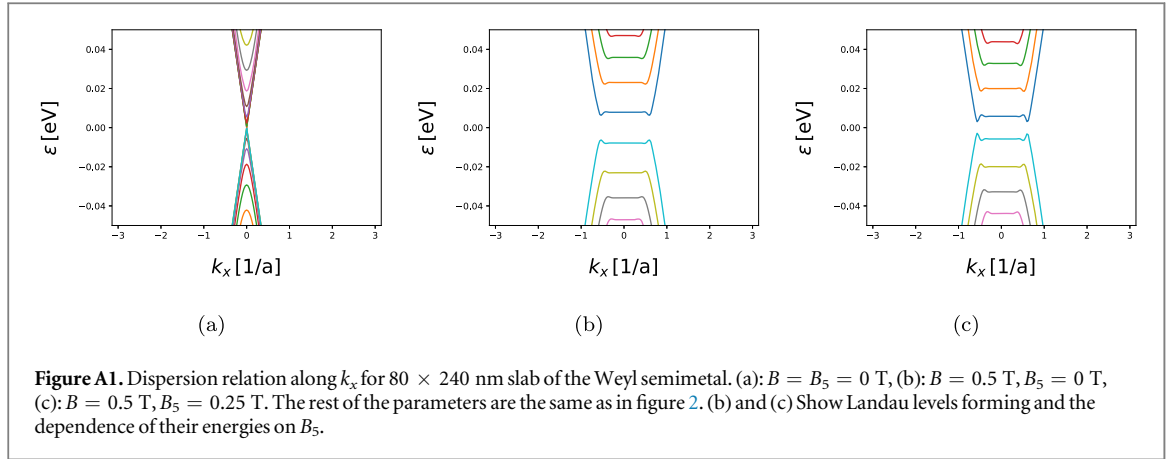To introduce a real magnetic field we use the standard Peierls substitution

$$t_x \longrightarrow e^{iBya/(h/e)} t_x, \tag{16}$$

which produces a real magnetic field in the z direction. With both real and pseudo-magnetic field present only x direction remains infinite in the simulations. Thus, even though the obtained agreement with the theory seen in figures 2 and 3 is very good, we could not get rid of the finite-size effects completely.

Discussion and outlook

In our numerical results we show DOS of a slab of the Cd_3As_2 for a fixed $B(B_5)$, while varying $B_5(B)$ correspondingly. This allows us to model the two experimental scenarios. We imagine putting a sample into fixed external field and continuously bending it to create the pseudo-magnetic field (see figure 3 for the change in DOS, corresponding to this scenario). Alternatively, one can fix the bend of the sample and change the external field (see figure 2 for similar results in this case). We show the result of the equation (10) *without fitting parameters* together with the numerically computed DOS. There is visible disagreement for small B_5 regime seen in figure 2, as the traverse of the Fermi arc is the relatively large part of the trajectory. The linear dependence of the trajectory length in (9) on the chemical potential is a simplistic approximation for the motion along Fermi arc, thus causing discrepancy. The good agreement otherwise shows reliability of our model for predicting the influence of the external and pseudo-fields. Thus our prediction enable extraction of the values of B_5 as a function of strain applied to material by applying external magnetic field and measuring SdH or dHvA quantum oscillations.

We stress that results presented here apply both to time-reversal- and inversion-broken WSM, since one can think of the latter as two time-reversed copies of the former. While locally the pseudo-CME might add up to a zero net contribution in time reversal symmetric systems due to the cancellation between time reversed pairs of nodes, the trajectories are still modified by them, and the effect on quantum oscillations should still be present.

Figure A1. Dispersion relation along k_x for 80×240 nm slab of the Weyl semimetal. (a): $B = B_5 = 0$ T, (b): $B = 0.5$ T, $B_5 = 0$ T, (c): $B = 0.5$ T, $B_5 = 0.25$ T. The rest of the parameters are the same as in figure 2. (b) and (c) Show Landau levels forming and the dependence of their energies on B_5.

The case of Dirac semimetals is more subtle: it is known that the strain can develop spin–orbit coupling gapping out the Dirac semimetals like Cd_3As_2, as the symmetry protecting the cones is broken [40, 41]. Nevertheless, we predict that small B_5 is still accessible in the experiment in the limit of high magnetic field or high chemical potential with respect to Dirac point compared to spin–orbit gap. In the first case the two Weyl cones corresponding to the same Dirac cone have opposite spins, and are shifted in energy and momentum due to Zeeman term (neglected so far, since it has a trivial effect of shifting the oscillations in energy for the two-node WSM). Thus, we predict two sets of quantum oscillations corresponding to the two spin sectors to be present. In the second case the gap near the Dirac points does not influence the physics at high chemical potential and our predictions remain intact. We note that the two sets of oscillations should be distinguishable in the experiment, similar to the purely bulk and bulk-boundary sets of oscillations in [25]. We also notice that the movement of one set of the oscillations with applied strain would help to clearly distinguish their bulk-boundary nature from the bulk set of quantum oscillation or more exotic phenomena like magnetophonon oscillations [42, 43].

Acknowledgments

Appendix

A.1. Dispersion relation
To corroborate the findings of the main text, here we present the dispersion relations for $B = B_5 = 0$ T; $B = 0.5$ T, $B_5 = 0$ T; and $B = 0.5$ T, $B_5 = 0.25$ T in figures A1(a)–(c) correspondingly.

A.2. Changes in the total arc length
In this section we consider the generic case in which the total length of the Fermi arcs is modified by the existence of a bulk B_5. This can occur, for example, in strained samples where strain is applied on one surface and gradually relaxes to zero away from that surface such that the opposite side of the sample maintains the original unstrained value.

Getting back to equation (9), we note that both L_{eff} and S_k depend on B, B_5, and L. Writing out S_k explicitly

$$2\pi(n + \gamma) = \mu(2L'/v + k_0(B_5)/evB) + k_0(B_5)\mu_0/evB. \tag{17}$$

where $k_0(B_5) = (k_0(0, B_5) + k_0(L, B_5))/2$, $k_0(z, B_5)$ is the Weyl node separation as a function of position in z direction and B_5. This expression transforms to equation (9) when $k_0(0) = k_0(L) = k_0$.

Let us now estimate the change in the overall arc length as follows. We assume that B_5 is uniform in the bulk of the sample, i.e the Weyl node separation changes linearly from one surface to another in the z direction. Hence the total arc length is given by

$$k_0(z, B_5) = k_0 + B_5(z - z_0), \tag{18}$$

where z_0 denotes the position in which the nodal separation is unperturbed. We set the sample position between $z = 0$ and $z = L$, so that $k_0(0, B_5) = k_0 - B_5 z_0$ and $k_0(L, B_5) = k_0 + B_5(L - z_0)$ and the change is the total length of the arcs can be estimated as $B_5(L - 2z_0)$ and is linear in B_5 and L.

Consequently, while we expect oscillations, they will not be at constant intervals as a function of B or B_5. We can consider the two limits of $B_5/B \gg 1$ and $B_5/B \ll 1$. For the latter, $L \approx L'$ and we get that

$$\Delta(1/B) = 2\pi e v/k_0(B_5)(\mu_0 + \mu) \tag{19}$$

the expression is of a similar form to the one appearing in [24], but now k_0 changes linearly in B_5. For $B_5 \gg B$ we have that $L' \approx LB_5/B$ so that

$$2\pi\hbar(n + \gamma) = \mu(2LB_5/vB + k_0(B_5)/evB) + k_0(B_5)\mu_0/evB \tag{20}$$

and therefore

$$\Delta(1/B) = 2\pi e v[2e\mu LB_5 + k_0(B_5)(\mu + \mu_0)]^{-1}. \tag{21}$$

And the denominator again changes linearly in both B_5, L.

A.3. Unisotropic Fermi velocity

In equation (1) the Fermi velocity was taken to have a constant and isotropic value, v. In practice, the Fermi velocity might have a different value depending on the direction, hence we now extend the calculation to the case where $\vec{v} = (v_\perp, v_\perp, v_z)$. Since we choose the direction of the external field to be in the z direction and perpendicular to the surface, we take the surface velocity to be $v_\perp$ as well. The modification introduced by the anisotropy affect equation (8), where v should be replaces by an effective velocity which is a combination of $v_\perp$ and v_z weighted by the magnitude of B and B_5, i.e

$$v_b = \sqrt{(\sin\theta v_\perp)^2 + (\cos\theta v_z)^2}, \tag{22}$$

where $\theta = \tan^{-1}(B_5/B) \equiv \tan^{-1}(x)$. v_b can be written as

$$v_b = [1 + x^2]^{-\frac{1}{2}}\sqrt{x^2 v_\perp^2 + v_z^2} \tag{23}$$

hence equation (8) becomes

$$\int \mathbf{p} \cdot \mathbf{dr} = 2L\mu\frac{1 + x^2}{\sqrt{x^2 v_\perp^2 + v_z^2}}. \tag{24}$$

The quantization condition (9) then becomes

$$2\pi(n + \gamma) = 2L\mu\frac{1 + x^2}{\sqrt{x^2 v_\perp^2 + v_z^2}} + \frac{k_0(B_5)(\mu + \mu_0)}{v_\perp eB}. \tag{25}$$

As expected, when $v_\perp$ and v_z are comparable, the same analysis that is presented in the main text holds. Alternatively, if one of these velocities is much larger than the other, the result depends on the magnitude of x and can show different dependencies on x. For example, if $v_\perp \gg v_z$ and $x \gg 1$, we find that

$$\frac{1 + x^2}{\sqrt{x^2 v_\perp^2 + v_z^2}} = \frac{1 + x^2}{v_\perp\sqrt{x^2 + (v_z/v_\perp)^2}} \approx \frac{x}{v_\perp}$$

while if $x \ll 1$ we have

$$\frac{1 + x^2}{\sqrt{x^2 v_\perp^2 + v_z^2}} = \frac{1 + x^2}{v_\perp\sqrt{x^2 + (v_z/v_\perp)^2}}.$$

The result in this case clearly depends on the hierarchy of x and $v_z/v_\perp$. For $x \gg v_z/v_\perp$ one gets $1/(v_\perp x)$, while for $x \ll v_z/v_\perp$ the result is $(1 + x^2)v_\perp/v_z$ as the lowest order correction in x.

References

[1] Peskin M E and Schroeder D V 1995 *An Introduction to Quantum Field Theory* (Reading, MA: Addison-Wesley)
[2] Volovik G E 2003 *The Universe in a Helium Droplet* (Oxford: Clarendon)
[3] Chiu C-K, Teo J C Y, Schnyder A P and Ryu S 2016 *Rev. Mod. Phys.* **88** 035005
[4] Burkov A, Hook M and Balents L 2011 *Phys. Rev.* B **84** 235126
[5] Wan X, Turner A M, Vishwanath A and Savrasov S Y 2011 *Phys. Rev.* B **83** 205101
[6] Turner A M, Vishwanath A and Head C O 2013 *Topological Insul.* **6** 293
[7] Armitage N, Mele E and Vishwanath A 2018 *Rev. Mod. Phys.* **90** 015001
[8] Fukushima K, Kharzeev D E and Warringa H J 2008 *Phys. Rev.* D **78** 074033
[9] Nielsen H B and Ninomiya M 1981 *Nucl. Phys.* B **193** 173
[10] Nielsen H and Ninomiya M 1983 *Phys. Lett.* B **130** 389
[11] Vazifeh M and Franz M 2013 *Phys. Rev. Lett.* **111** 027201
[12] Ma J and Pesin D 2015 *Phys. Rev.* B **92** 235205
[13] Son D T and Spivak B Z 2013 *Phys. Rev.* B **88** 104412
[14] Kim H-J, Kim K-S, Wang J-F, Sasaki M, Satoh N, Ohnishi A, Kitaura M, Yang M and Li L 2013 *Phys. Rev. Lett.* **111** 246603

[15] Burkov A 2015 *Phys. Rev.* B **91** 245157

[16] Huang X *et al* 2015 *Phys. Rev.* X **5** 031023

[17] Xiong J, Kushwaha S K, Liang T, Krizan J W, Hirschberger M, Wang W, Cava R and Ong N 2015 *Science* **350** 413

[18] Li Q, Kharzeev D E, Zhang C, Huang Y, Pletikosić I, Fedorov A, Zhong R, Schneeloch J, Gu G and Valla T 2016 *Nat. Phys.* **12** 550

[19] Arnold F *et al* 2016 *Nat. Commun.* **7** 11615

[20] Pikulin D, Chen A and Franz M 2016 *Phys. Rev.* X **6** 041021

[21] Grushin A G, Venderbos J W, Vishwanath A and Ilan R 2016 *Phys. Rev.* X **6** 041046

[22] O'Brien T, Beenakker C and Adagideli İ 2017 *Phys. Rev. Lett.* **118** 207701

[23] Potter A C, Kimchi I and Vishwanath A 2014 *Nat. Commun.* **5** 5161

[24] Zhang Y, Bulmash D, Hosur P, Potter A C and Vishwanath A 2016 *Sci. Rep.* **6** 23741

[25] Moll P, Nair N, Helm T, Potter A, Kimchi I, Vishwanath A and Analytis J 2016 *Nature* **535** 266

[26] Vozmediano M, Katsnelson M and Guinea F 2010 *Phys. Rep.* **496** 109

[27] Levy N, Burke S A, Meaker K L, Panlasigui M, Zettl A, Guinea F, Neto A H C and Crommie M F 2010 *Science* **329** 544–7

[28] Liu C-X, Ye P and Qi X-L 2013 *Phys. Rev.* B **87** 235306

[29] Chernodub M N, Cortijo A, Grushin A G, Landsteiner K and Vozmediano M A 2014 *Phys. Rev.* B **89** 081407

[30] Shapourian H, Hughes T L and Ryu S 2015 *Phys. Rev.* B **92** 165131

[31] Cortijo A, Ferreirós Y, Landsteiner K and Vozmediano M A 2015 *Phys. Rev. Lett.* **115** 177202

[32] Sumiyoshi H and Fujimoto S 2016 *Phys. Rev. Lett.* **116** 166601

[33] Chernodub M and Zubkov M 2017 *Phys. Rev.* B **95** 115410

[34] Nica E M and Franz M 2018 *Phys. Rev.* B **97** 024520

[35] Peri V, Serra-Garcia M, Ilan R and Huber S D 2019 *Nat. Phys.* **15** 357–61

[36] Ruan J, Jian S-K, Yao H, Zhang H, Zhang S-C and Xing D 2016 *Nat Commun.* **7** 11136

[37] Ilan R, Grushin A G and Pikulin D I 2020 *Nat. Rev. Phys.* **2** 29–41

[38] Abrikosov A 2017 *Fundamentals of the Theory of Metals* (New York: Dover)

[39] Liu T, Pikulin D I and Franz M 2017 *Phys. Rev.* B **95** 041201

[40] Wang Z, Sun Y, Chen X-Q, Franchini C, Xu G, Weng H, Dai X and Fang Z 2012 *Phys. Rev.* B **85** 195320

[41] Wang Z, Weng H, Wu Q, Dai X and Fang Z 2013 *Phys. Rev.* B **88** 125427

[42] Raichev O. E. 2016 *Phys. Rev.* B **94** 121201

[43] Kumaravadivel P. *et al* 2019 *Nat. Commun.* **10** 3334

[44] Groth C W, Wimmer M, Akhmerov A R and Waintal X 2014 *New J. Phys.* **16** 063065